



TECHNICAL ARTICLE

Fabrication, Characterization, and Corrosion Protection of Siloxane Coating on an Oxygen Plasma Pre-treated Silver-Copper Alloy

Yasmin A. El-Moaz, Wafaa A. Mohamed, Mai M. Rifai, Nasser N. Morgan, Khaled H. Metwally, and Nabil A. Abdel Ghany

Submitted: 18 September 2022 / Revised: 3 January 2023 / Accepted: 24 January 2023 / Published online: 13 March 2023

In this study, siloxane has been used for the protection of metal artifacts from corrosion in the form of transparent barrier coating films because of their good adhesion to the metal substrate. The effect of oxygen plasma pre-treatment on the adhesion properties of the siloxane thin film on the silver-copper alloy substrate was investigated. Radiofrequency plasma-enhanced chemical vapor deposition (RF-PECVD) was used for the deposition process. Surface identification and characterization of the deposited films were carried out using Scanning Electron Microscopy coupled with energy-dispersive x-ray spectroscopy (SEM-EDX) and Fourier-transform infrared spectroscopy (FT-IR). Surface topography and roughness were investigated by atomic force microscopy (AFM). The hydrophobic characteristic was measured by water contact angle measurement (WCA). The film thickness was evaluated using a spectroscopic ellipsometer (SE). Colorimetric measurement (CM) was used to evaluate changes in the appearance of the surface following the PECVD deposition of the SiO₂ protective layer. The corrosion protection ability of siloxane films for metal substrates as a function of RF power and gas feed composition was examined by the electrochemical impedance spectroscopy (EIS) technique. It was found that the deposited film improved the protective efficiency for samples from 55.29 to 92.93%. Besides, after the oxygen plasma pretreatment step, the film showed better corrosion resistance of the tested samples.

Keywords cold plasma, corrosion protection, PECVD, siloxane, silver-copper artifacts, surface modification, thin-film

Abbreviations

CH	Cultural heritage
RF-PECVD	Radiofrequency plasma enhanced chemical vapor deposition
SEM-EDX	Scanning Electron Microscopy coupled with energy-dispersive x-ray spectroscopy
AFM	Atomic force microscopy
WCA	Water contact angle
FT-IR	Fourier-transform infrared spectroscopy
SE	Spectroscopic ellipsometer
CM	Colorimetric measurement
EIS	Electrochemical impedance spectroscopy

1. Introduction

Silver has been a precious and valuable metal in many ancient cultures due to its aesthetic appeal, and can be found in both cultural heritage and private collections in abundance (Ref 1, 2). Since tarnish on silver artifacts is mostly caused by hydrogen sulfide (H₂S), a frequent contaminant, silver artifacts should be kept away from environments with aggressive species (Ref 3). The choice of an appropriate protection strategy can only be made with complete knowledge of the corrosion processes under the given circumstances (Ref 4). High-temperature resistance, strong strength, thermal fatigue, chemical inertness, a low friction coefficient, and affordability

should all be requirements for high-quality coatings (Ref 5). One of the easiest and most effective ways to safeguard metals and alloys is to coat them with a polymer that will not react with the material (Ref 6). Coatings can be applied to a wide variety of substrate materials that undergo a variety of chemical treatments; therefore, it is important to zero in on the least interceptive approach that provides the best surface for adhesion (Ref 7). The use of non-thermal plasma procedures to safeguard metals has been advocated as an alternative to the more traditional approaches, which are occasionally linked to major environmental concerns (Ref 8, 9). Those who work to preserve cultural artifacts have taken notice of this method because of how low the temperature is (Ref 10-14). A non-thermal plasma is a partially ionized gas in which high-energy

Yasmin A. El-Moaz, Wafaa A. Mohamed, and Mai M. Rifai, Conservation Department, Faculty of Archaeology, Cairo University, Giza 12613, Egypt; **Nasser N. Morgan**, Plasma Center, Al-Azhar University, Cairo 11884, Egypt; and **Physics Department, Faculty of Science, Al-Azhar University, Cairo 11884, Egypt**; **Khaled H. Metwally**, Physics Department, Faculty of Science, Al-Azhar University, Cairo 11884, Egypt; and **Nabil A. Abdel Ghany**, Physical Chemistry Department, Electrochem. and Corrosion Lab, National Research Centre, Dokki 12622 Cairo, Egypt. Contact e-mails: yasmin97@cu.edu.eg, na_manakhly@yahoo.co.uk, and na.abdelghany@nrc.sci.eg.

electrons are mixed with low-energy molecular species (ions, free radicals, metastable excited species, etc.) to keep the temperature of the system relatively stable, usually around room temperature. Low-pressure radio frequency plasma-enhanced chemical vapor deposition (RF-PECVD) has a reasonably high plasma density, which promotes the gas-phase production of particulate matter necessary for producing corrosion-resistant coatings with organized rough surfaces (Ref 15, 16). Plasma treatment is not a simple task, but rather a “field of opportunities” (Ref 17) because it allows pretreatments of the substrate before the deposition to remove a contaminated layer, oxidize or reduce the surface, or seed specific chemical species (like F atoms) (Ref 8, 18, 19). Depending on the plasma mode, the choice of the precursors, and the discharge circumstances, cold plasma can have a variety of effects on substrates (Ref 16, 20, 21). Organic contamination on the substrate’s surface is reacted with by reactive plasma species, which enhance the substrate’s adhesion characteristics (Ref 7). These organic contaminants frequently consist of hydrocarbons that are not tightly bonded. Oxygen, hydrogen, and carbon all react, releasing H₂O and CO₂ from the surface of the substrate. Plasma grafting and cross-linking of chemical functionalities are performed in inert or reactive gases, such as Ar, H₂, CO₂, NH₃. (Ref 19, 22). Hexamethyldisiloxane (HMDSO) ([CH₃]₃SiOSi[CH₃]₃) is still the most frequently employed organosilicon compound for waterproof coatings (Ref 23-26). Polymers of organic silicon and their compounds are typically non-toxic, extremely simple chemicals that are widely employed in numerous technical domains. Thin organic silicon coatings can exhibit a range of traits since they are both inorganic and organic, including abrasion resistance, anti-reflective qualities, thermal stability, dielectric properties, and adjustable hydrophilic or hydrophobic properties (Ref 19, 27, 28). Clusters are created after HMDSO polymerizes as a result of plasma treatment. With their substantial static water contact angles, these clusters offer good waterproof characteristics (Ref 29).

The current study aims to compare how protective thin films made of HMDSO/O₂ grow on silver-copper alloy substrates that have already been treated and those that have not been treated. Additionally, investigate oxygen plasma pretreatment, which eliminates organic contamination from the surface and

creates a buffer layer by catalyzing active points, enhances the adhesion of the coating to the substrate and increases the level of surface oxidation. Accordingly, the most important aspect of this work is to clarify that the modifications in the plasma processing parameters have a significant impact on the corrosion protection of the produced SiO_x thin films on silver-copper alloy substrates. Along with demonstrating the crucial role O₂ gas plays in the pretreatment. The EIS technique is used to examine the coating films to figure out how well they protect the metal from corrosion.

2. Experimental Procedure

2.1 Materials

A silver-copper alloy with the following composition (wt.%: Ag 85, Cu 15) was cast into a closed mold. It was then cold rolled to a thickness of 0.3 mm. The rolled sheet was cut into 20 × 20 mm coupons [18]. In accordance with ASTM guidelines, all coupons were cleaned and then kept for a number of days in a desiccator, wrapped in optical paper [30]. Commercial O₂ gas and HMDSO ([CH₃]₃SiOSi [CH₃]₃) (Sigma-Aldrich) with 98% purity were used as received without further purifications.

2.2 Plasma Deposition Reactor

Figure 1 Provides a schematic illustration of the RF-plasma CVD process that was employed to produce SiO₂. It comprises a stainless steel chamber that is 20 cm long and 10 cm in diameter. Two stainless steel electrodes with a diameter of 5 cm each are installed in the chamber. Teflon flanges separated these electrodes from the chamber wall.

A fixed separation of 5 cm between the power electrode and ground electrode has been used during the deposition process RF power supply (Coaxial power UK model RFG 1 K-13) with (13.56 MHz) according to EN ISO 9001 standards, a π type matching network with two variable air gap capacitors with values between 0 and 250 pF and an air variable coil is used to supply 1 kW of power to the chamber. Throughout the experiment, the reflected power was kept at zero.

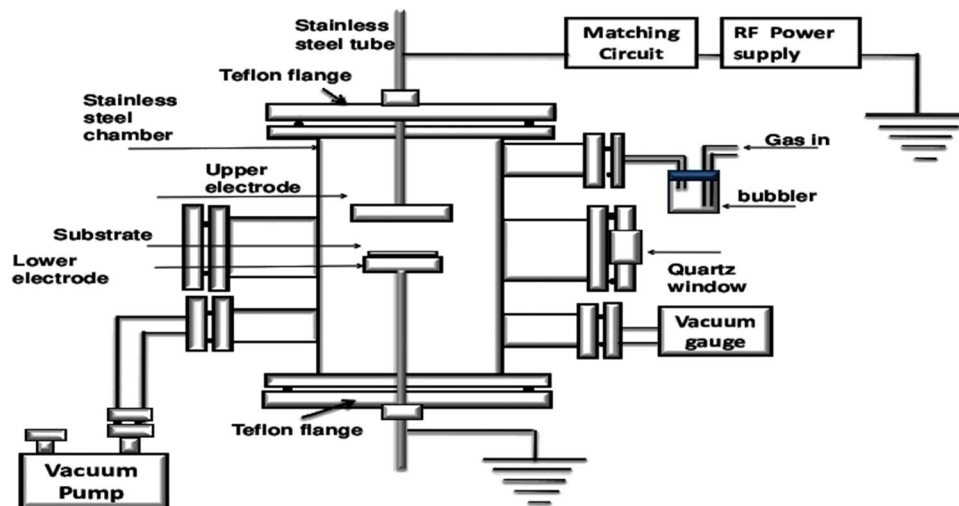


Fig. 1 shows a schematic of the RF-PECVD experimentation equipment used for film deposition

Table 1 Summary of experimental conditions of PECVD of SiO₂ films

Sample	Deposition power, W	Time of pre-treatment, min	deposition time, min	Gas for pretreatment at 100 W and 1000 mTorr	Carrier gas for deposition
Blank (bare substrate)
Pre-activated sample with oxygen plasma before deposition	100	3	...	Oxygen	Oxygen
Deposited samples without pre-activation with O ₂ plasma (A)	100	...	5	...	Oxygen
Deposited samples without pre-activation with O ₂ plasma (B)	200	...	5	...	Oxygen
Deposited samples after activation with O ₂ plasma (C)	100	3	5	Oxygen	Oxygen
Deposited samples after activation with O ₂ plasma (D)	200	3	5	Oxygen	Oxygen

First, the reactor was evacuated to a pressure of 60 millitorrs. Next, oxygen was used as a carrier gas while HMDSO vapor was pumped into the chamber through a stainless steel bubbler. The overall pressure of the discharge cell ranged between 0.2 and 3 Torr in this chamber, which is operating at a moderate vacuum. The samples were processed on the grounded electrode at the floating temperature that the plasma attained ($T < 70\text{ }^{\circ}\text{C}$), and the pressure was fixed at the desired value using a needle valve and pressure gauge. This was done by RF energy on a gas combination that includes oxygen and hexamethyldisiloxane (HMDSO) with a feed composition of approximately 2 sccm. HMDSO precursor is used more easily in vapor deposition procedures since it is non-toxic, non-explosive, and gives a transparent thin film. Because it has the Si-O linkages required for the creation of silicon oxide thin films, using this monomer is favorable. The substrates were pre-treated with O₂-plasma at 100 W and 1000 mTorr before deposition. The total pressure during the deposition step is 300 mTorr. The experimental conditions are reported in Table 1.

2.3 Characterization Techniques

Chemical characterization of the deposited films was performed on a JASCO FT-IR- 460 plus Spectrometer in reflection mode by using attenuated total reflectance, 400 and 4000 cm⁻¹ (ATR). Morphological characterization was performed before and after deposition utilizing a scanning electron microscope: Model Zeiss Sigma 300 VP Field Emission Gun (FEG), stability > 0.2%/h. attached to an EDX Unit (Smart EDAX- energy-dispersive spectroscopy (EDX)- line ID), with accelerating voltage 0.02-30 kV, with resolution up to 3072 × 2304 pixels. The FESEM.EDX was performed at the Egyptian Petroleum Research Institute, Nasr City, and Cairo, Egypt.

Morphological, topographical characteristics and the roughness of the films deposited on the silver alloy substrates were measured using an atomic force Microscope Auto probe cp-research head manufactured by Thermo microscopes operated in contact mode using a Silicon Nitride Probe Model MLCT manufactured by Broker. The scan settings were adjusted with the help of Proscan 1.8 software. IP 2.1 software was used for the analysis of the scanned images (contact mode, scan area of 2.5 × 2.5 μm², the scan rate of 1 Hz, and a number of data points 256 × 256 points).

The efficiency of the protective SiO_x film was assessed using electrochemical impedance spectroscopy (EIS). Electrochemical impedance measurements were performed in an aerated 0.1 M NaCl solution at a laboratory temperature of 25 °C ± 1. The test was conducted in a three-electrode electrochemical cell connected to a Potentiostat/Galvanostat, AUTO LAB 302N, with FRA32, the Netherlands. Saturated silver/silver chloride was used as a reference electrode, a platinum mesh as an auxiliary electrode and the metal sample as a working electrode. Impedance spectra were recorded at Potential (V) linked with O.C.P. (Open Circuit Potential, 30 min) value in the frequency range 5000-0.02 Hz.

By measuring the contact angle, the hydrophobic or hydrophilic properties of the deposited layer were evaluated to figure out how well the surface would hold water using deionized water as a liquid probe by utilizing a Compact Video Microscope CVM 130 X. The colorimetric measurement assisted in determining the resistance of a SiO₂ PECVD deposition to tarnishing both visually and quantitatively using Miniscan Ez portable color measurement spectrophotometer: The MSEZ-4500S operates with a d/0 SCE measuring geometry, has a measured area of less than Ø6 mm, and excludes the specular component (SCE). The film thickness has been evaluated using a Spectroscopic Ellipsometer PHE-103 Angstrom Ellipsometer, as the sample is measured at the range from 400 to 700 nm and an angle of incidence of 70°. After the measurement, data fitting analysis was performed using the fitting algorithms and mathematical modeling to determine the film thickness.

3. Results and Discussion

3.1 FT-IR Analysis

FT-IR data are recorded in Fig. 2, and the assignment of characteristic wave numbers is listed in Table 2.

The most important characteristic bands in the FTIR spectra of the precursor (HMDSO) are 2922-2961 cm⁻¹ (asymmetric stretching in CH₃ groups), 1260 cm⁻¹ (Si-CH₃ wagging (symmetric bending of methyl groups bonded to Si)), 849 cm⁻¹ (rocking of CH₃ in Si-((CH₃)₃)), and 1072 cm⁻¹ (rocking of CH₃ in Si-((CH₃)₃) (Si-O-Si asymmetric stretching (Ref 31)).

As illustrated in Table 1 and Fig. 2, a few characteristics can be seen in the spectra of the deposited coupons with various parameters: Other typical Si-O rocking and bending absorption bands are located at 450 cm⁻¹ and 800 cm⁻¹, respectively, as well as the Si-O-Si asymmetric stretching absorption bands at 1000-1150 cm⁻¹.

The FTIR absorption spectra of samples A and C showed the absorption bands of Si-O at 1040 cm⁻¹, 1059 cm⁻¹ (stretching) and 802 cm⁻¹, and 797 cm⁻¹ (bending), respectively. Organic groups were detected in coupons A and C such as C-H asymmetric stretching at 2922 cm⁻¹, and 2917 cm⁻¹, respectively.

Si-CH₃ wagging or symmetric bending of methyl groups bonded to Si was detected for sample A at 1278 cm⁻¹. Also surface Si-OH groups situated were detected for samples A and C at 3312 cm⁻¹, and 3329 cm⁻¹, respectively. The features of silanol groups (Si-OH) were detected for samples A and C at 933 cm⁻¹, and 925 cm⁻¹ (bending), respectively.

The FTIR absorption spectra of samples B and D showed the absorption bands of Si-O at 1044 cm⁻¹, 1026 cm⁻¹ (stretching) and 817 cm⁻¹, 804 cm⁻¹ (bending), respectively, while organic groups were not detected.

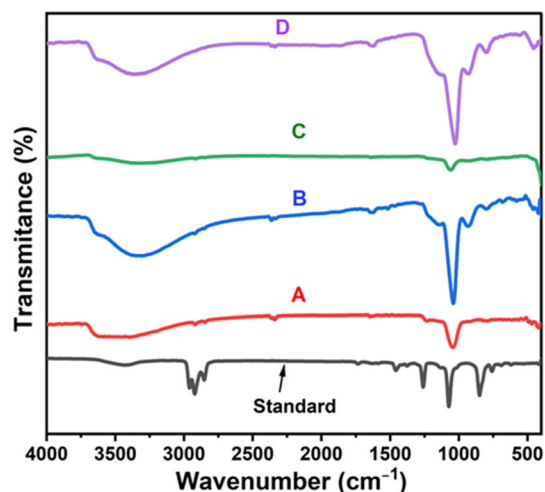


Fig. 2 FTIR transmittance spectra of the standard precursor (HMDSO) and the deposited samples A, B, C and D

The low intensity of the CH_x symmetric and asymmetric stretching bands at 2900-2960 cm⁻¹, as well as the absence of other typical CH_x bands like the Si-CH₃ rocking vibration at 840 cm⁻¹ and the CH₃ symmetric bending in Si-CH₃ at 1260 cm⁻¹, provided further confirmation of the low carbon content and consequently SiO₂-like nature of the deposited films of sample Band C. Surface Si-OH groups situated and silanol groups Si-OH stretching absorption bands were not detected for sample D but Si-OH groups absorption bands were detected for sample B at 3395 cm⁻¹.

By removing organic groups from the formed thin film, FTIR analysis results show that increasing input power has a significant impact on the chemical composition of coatings (Ref 20, 26). Additionally, after being briefly exposed to active plasmas like oxygen plasma, the substrate develops reactive sites that can be used to plasma polymerize the precursor molecule later on to create covalent bonds between the substrate and the deposition layer (Ref 32). Also, the oxygen atoms made by the plasma action “burn” the organic groups, leaving behind a layer of inorganic siloxane (Ref 33-35). In general, the strength of Si-related absorptions increases with the coating’s Si content, which is not always proportional to the coating’s thickness but rather to the degree of “inorganication” and the presence of SiO_x inclusions (Ref 26, 34, 35).

3.2 SEM and EDX Analyses

The results of SEM and EDX analyses showed the surface morphology and analysis of the samples as follows: Fig. 3 shows the surface of the silver-copper alloy substrate before pretreatment, whereas Fig. 4 represents the substrate after deposition without pre-activation with oxygen plasma, whereas Fig. 5 reveals the deposited film on the sample after activation with oxygen plasma.

The untreated samples with oxygen plasma before deposition showed poor adhesion and homogeneity between the deposited thin film and the irregular surface of the silver alloy substrate, Fig. 4. The substrate and the corrosive environment can communicate directly through the porosities and pinholes in coatings. While the pre-activated substrate with oxygen plasma deposited with O₂/HMDSO mixtures covered the irregular defects of the substrate surface, this deposited thin film covered the surface uniformly and had a high degree of adhesion and adaptability to the surface morphology, as shown in Fig. 5.

Table 2 FT-IR peak wave numbers and vibrational assignments detected in the analyzed experimental samples

Vibrational assignment	wave numbers cm ⁻¹	standard precursor, HMDSO	Sample A	Sample B	Sample C	Sample D
<i>Inorganic groups</i>						
Si-OH groups	3300-3400	n.d	3312	3395	3329	n.d
Silanol groups Si-OH stretching	900-920	n.d	933	919	925	n.d
Si-O-Si asymmetric stretching vibration mode	1000-1150	1072	1040-1134	1044	1059	1026
Si-O-Si bending vibration mode	800	849	802	817	797	804
Si-O-Si Rocking mode	450	450	422	416	n.d	454
<i>Organic groups</i>						
C-H asymmetric stretching	2900-2960	2922-2961	2922	n.d	2917	n.d
Si-CH ₃ wagging (symmetric bending of methyl groups bonded to Si)	1260	1259	1278	n.d	n.d	n.d
rocking of CH ₃ in Si-((CH ₃) ₃)	850	849	n.d	n.d	n.d	n.d

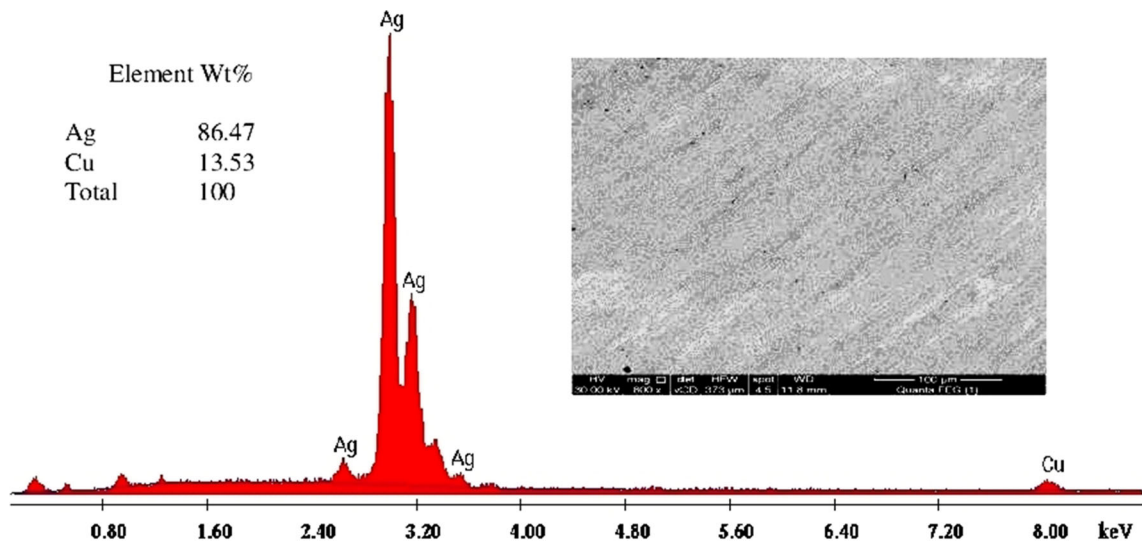


Fig. 3 The surface of the silver-copper alloy substrate before pretreatment

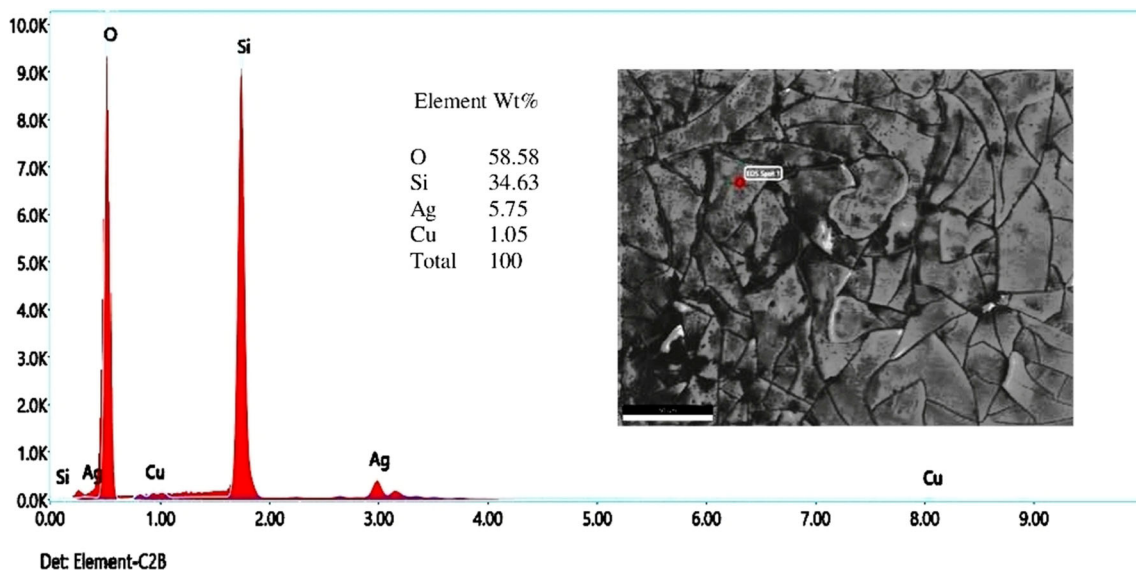


Fig. 4 The substrate after deposition without pre-activation with oxygen plasma

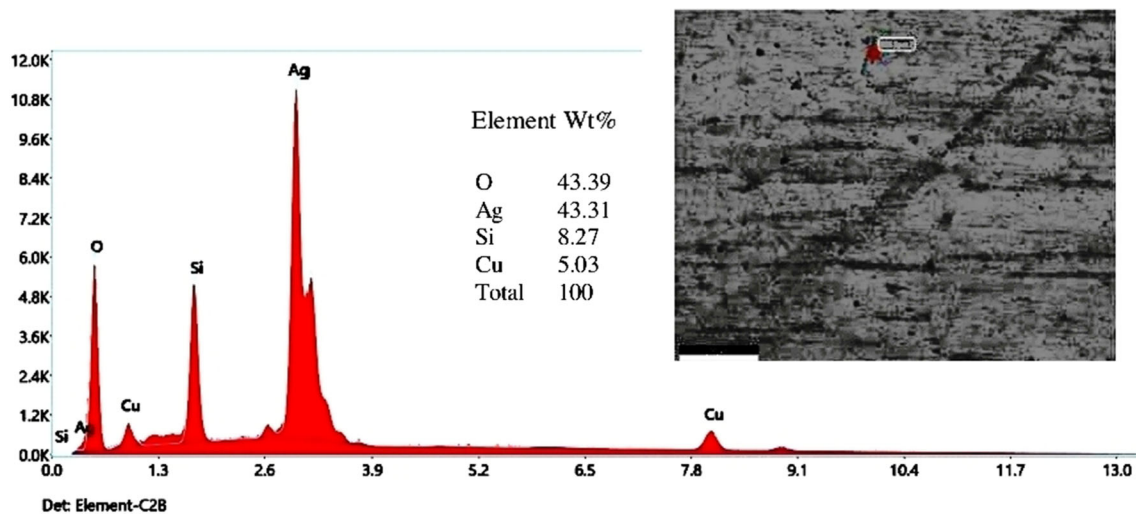


Fig. 5 Shows the deposited film on the sample after pre- activation with oxygen plasma

According to the findings of the SEM-EDX research, pre-activation plays a crucial role in ensuring that there is a specific concentration of polar functional groups, which will ultimately ensure that a uniform coating adheres well (Ref 35). Plasmas are useful for cleaning up organic smudges on inorganic surfaces. Non-polymerizable gases are commonly used in plasma treatments of metals to produce ultra-clean surfaces that produce stronger bonding than conventionally cleaned surfaces. The majority of the surface modifications are caused by the free radicals produced by low-pressure gas plasmas. The main factor contributing to better bonding to plasma-treated surfaces is the elimination of carbonaceous impurities. Strong boundary layers can be removed using plasma etching, a significant pretreatment alternative to conventional solution cleaning (Ref 18, 36).

3.3 Contact Angle Measurements

When dealing with corrosion protection, characterization of surface energy is an important issue, and measuring the water contact angle test is required. Measurements of water contact angles showed that the bulk coupon's contact angle was 72°, while after deposition it ranged between 75° and 79° for samples A and C, respectively. Samples B and D, on the other hand, ranged between 83° and 105°, as shown in Fig. 6 as well as Table 3.

Water contact angle measurements demonstrated that the addition of oxygen to the surface produced silanol groups, which increased the surface energy's polar component and

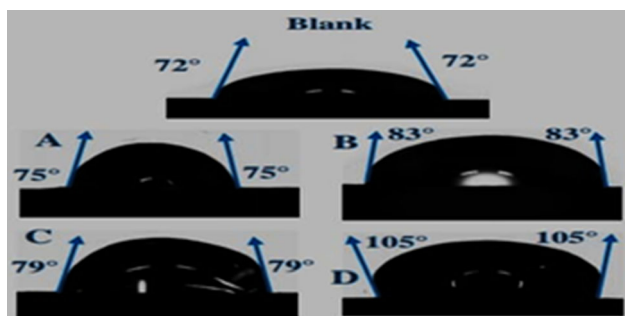


Fig. 6 Contact angles for the blank sample and the deposited samples without pre-activation with oxygen plasma (A and B) and samples with pre-activation with oxygen plasma (C and D)

Table 3 Physical characteristics of samples

Sample	ΔE	Rough, Rms, nm	Ave Rough, Ra, nm	Contact angle, θ , deg	Coating thickness, nm	protective efficiency %
Blank (bare substrate)	11.52	35.79	30.39	72
Pre-activated coupon with oxygen plasma before deposition	...	34.37	26.55
Coupons without pre-activation and deposited with oxygen plasma						
A	5.22	58,14	46,98	75	...	55.29%
B	4.46	33.59	26.50	83	939.53	92.93
Coupons with pre-activation and deposited with oxygen plasma						
C	4.64	75,60	58,67	79	...	78.72
D	3.25	47,59	35,36	105	955.27	93.38

reduced the contact angle to 75° and 79° for samples with less input power (100 W). On the other hand, when the input power was increased to (200 W) the contact angle ranged from 83 to 105°.

3.4 AFM Analyses

AFM 2-dimensional and 3-dimensional micrographs of the blank sample revealed an inhomogeneous surface with an average roughness (Ra) of 30.39 nm (Fig. 7(a), (b)). Samples A and B, which were not pre-activated and deposited with oxygen plasma, produced inhomogeneous films with Ra values of 46.98 and 26.50 nm, respectively, (Fig. 7(c)-(f) and their films contained both large and small particles (Fig. 8).

Figure 9(a), (b) represents the blank sample after pre-activation with oxygen plasma, which caused a decrease in the surface roughness (Ra values of 26.55 nm) and an improvement in the adhesion between the substrate and the deposited thin film.

Sample C, which was pre-activated and deposited with oxygen plasma at a power of 100 w, produced a surface with high roughness (Ra values of 58.67 nm), and the size of its particles was measured as shown in Fig. 10. The sample D, which was pre-activated and deposited with oxygen plasma at power 200 w produced a homogenous surface texture (Fig. 9e, f) with Ra values of 35.36 nm and the formation of regular, orderly clusters as shown in Fig. 11.

As a result, depending on the deposition conditions, the composition and morphological structure of the deposited films alter and affect the gas barrier performance (Ref 36), also pointed out the role of the high power of 200 W in decreasing the roughness of the coated sample to (rms values of 26.50 nm) better than the power of 100 W, which raises the roughness to (rms values of 46.98) for the deposited sample without pre-activation with oxygen plasma. In addition, it decreases the roughness of the deposited sample after activation with oxygen plasma from Ra values of 58.67 to 35.36 for sample C at power 100 and sample D at power 200, respectively, as shown in Table 3.

For the pre-activated samples with oxygen plasma, AFM examination revealed that the surface was uniformly covered in SiO₂-like layers and that it is distinguished by good adaptation to the underlying substrate, especially for coupons that are deposited under a power of 200 W as shown in Fig. 9. These results revealed the role of pre-activation or modification by oxygen plasma before deposition, as the pre-treatment step strongly decreases surface roughness to (rms values 26.55 nm)

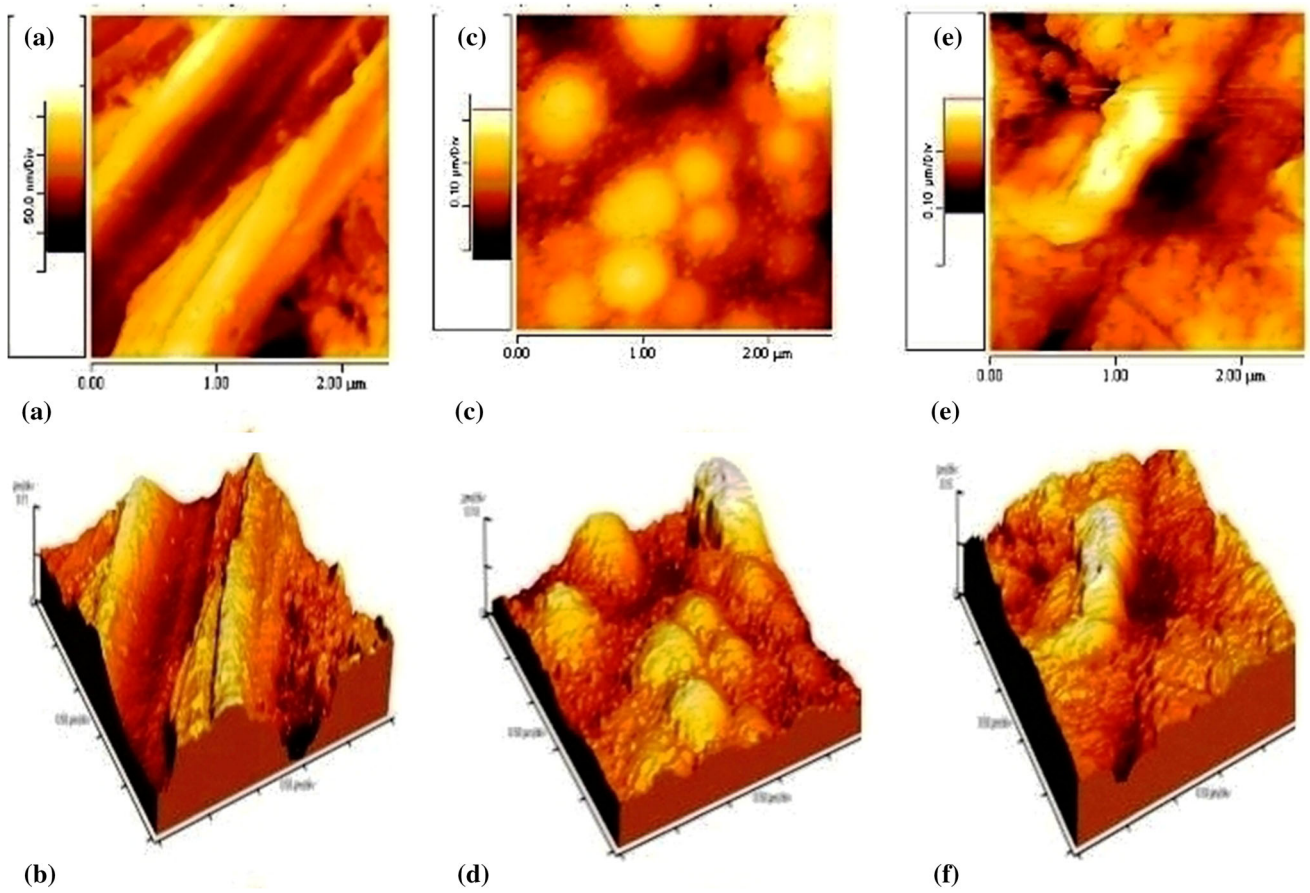


Fig. 7 Inhomogeneous surface of the blank sample (a and b) and samples without pre-activation with oxygen plasma, A (c and d) and B (e and f)

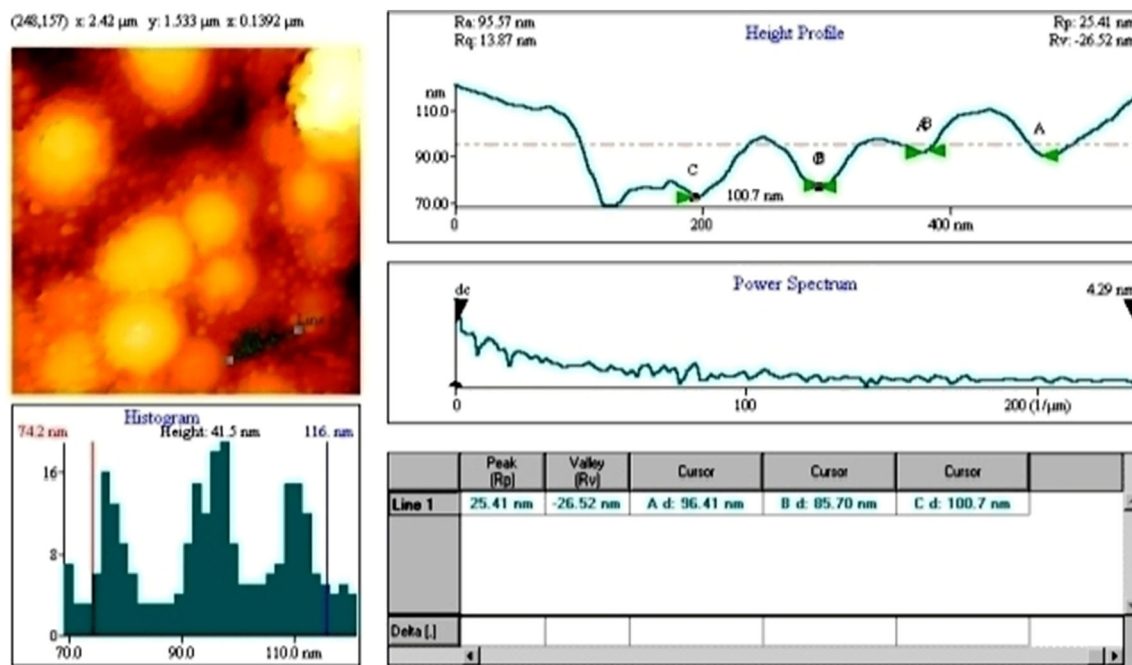


Fig. 8 Sample B showed the presence of different sizes of particles ranging between small and large particles

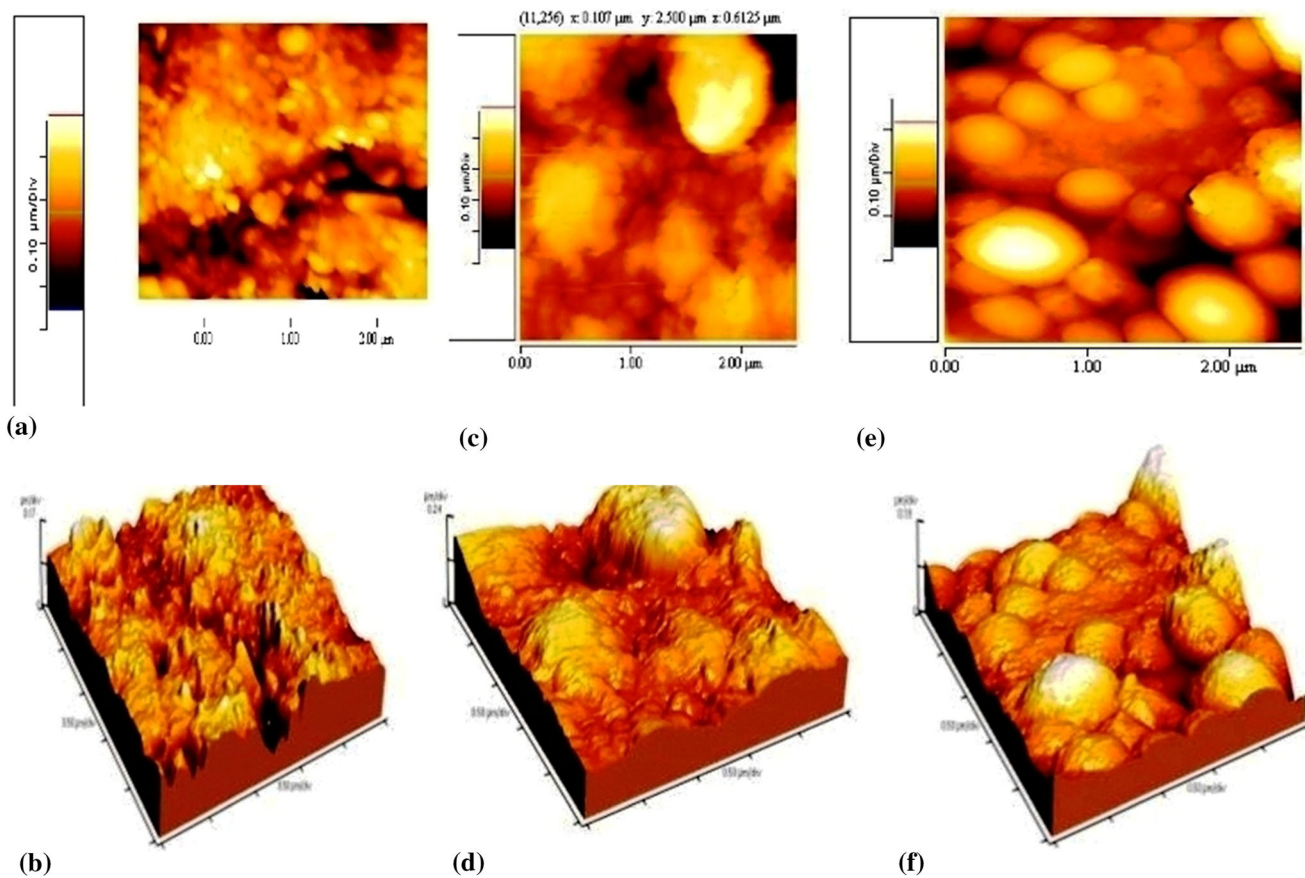


Fig. 9 The blank sample after pre-activated with oxygen plasma (a and b) and samples with pre-activation and deposited with oxygen plasma, C (c and d) and D (e and f)

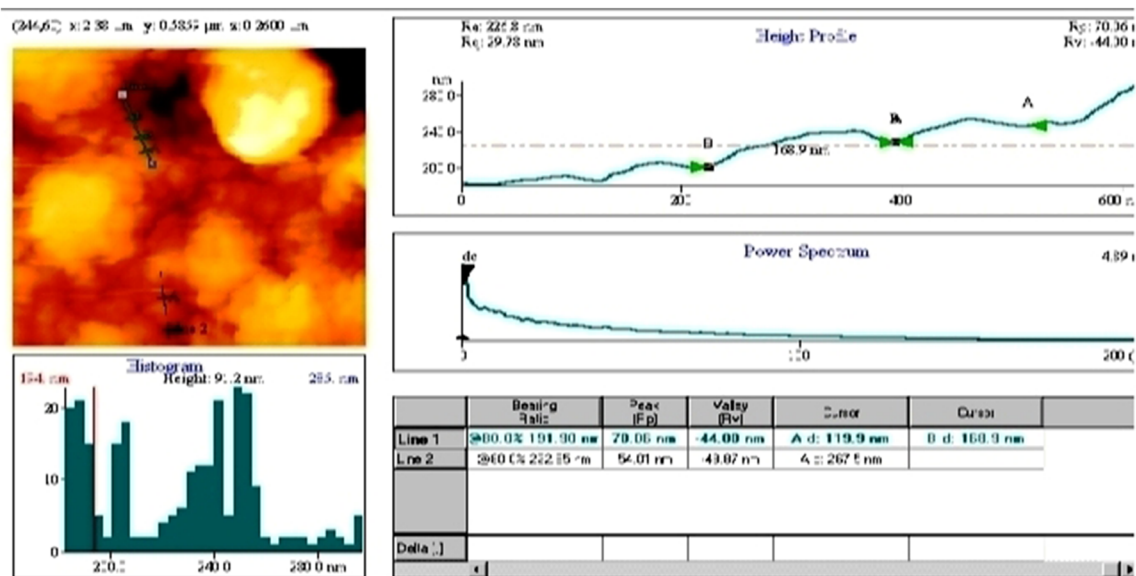


Fig. 10 Sample C showed the presence of different sizes of particles

and improves the adhesion between the substrate and the deposited thin film as shown in Fig. 9(a) and (b).

Particle creation suggests that the plasma polymerization in the gas phase was the preferred plasma polymerization at the

surface of the growing film when using high power and treating the surface. The surface electrostatic charge may attract the big particles, which could then be integrated into the film (Ref 8, 37).

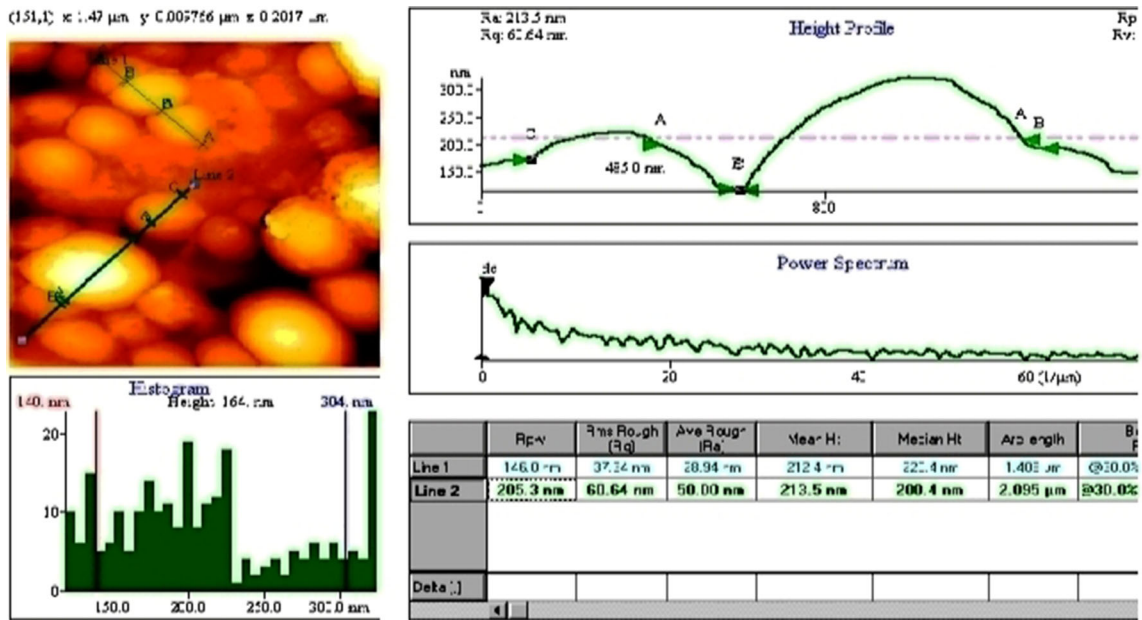


Fig. 11 Sample D showed the presence of the organized particles in the deposited film

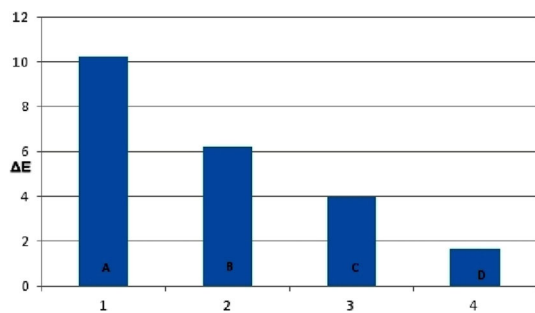


Fig. 12 Showed the results of color change measurements (ΔE^*) for the blank sample and the all different parameters of the deposited samples

The SiO_2 layer's resistance to tarnishing was greatly improved by the PECVD deposition of the SiO_2 , as evidenced by optical observation and quantitative colorimetric studies. Tarnishing susceptibility was assessed by estimating the average of (ΔE^*) after accelerated aging of the blank and coated samples. The tarnishing test was performed by exposing the samples to a saturated sulfide atmosphere with a simple corrosion test performed at 90% relative humidity. The samples were placed in desiccators with 0.5 g/l sodium sulfide solution and a saturated potassium sulfate solution to increase the relative humidity to 97.3% for 24 h [38]. According to color change measurements (ΔE^*) for the reference samples and the all different parameters of the deposited samples Fig. 12 and Table 4 showed that: $A > B > C > D$.

The result of color change measurement of the coated samples revealed that samples D, C and B gave the best results as they displayed the least average of ΔE 1.65, 3.97 and 6.22, respectively, whereas sample A displayed the highest average of ΔE 10.21. These results emphasize the role of pretreatment with oxygen plasma and the high power of the deposited film to protect the silver-copper alloys.

Table 4 Shows ΔE of the reference samples and Samples after aging

Sample	Reference sample			Sample after aging			ΔE
	L^*	a^*	b^*	L^*	a^*	b^*	
A	38.24	0.09	1.27	45.83	3.89	20.90	10.21
	36.74	3.59	1.97	45.83	1.50	10.45	
B	49.08	0.21	4.01	43.56	0.70	5.14	6.22
	33.90	6.26	10.20	42.09	0.86	0.81	
C	48.77	2.5	7.56	48.14	3.1	4.46	3.97
	41.73	1.95	5.28	41.73	2.3	2.13	
D	56.28	0.87	5.43	54.04	0.55	8.95	1.65
	53.19	1.91	12.52	55.58	0.36	11.71	

3.5 EIS Measurements

The corrosion protection of the deposited thin film coating on the metal substrate in 0.1 M NaCl solution was investigated using electrochemical impedance spectroscopy (EIS). By analyzing the extracted results, they provided information about the interactions that occur at the interface between the metal surface and the electrolyte solution. The increase in the amount of electrolyte that penetrates the coating indicates weak corrosion protection. Figure 13 shows the classical model used to simulate the coating/substrate systems (Ref 39). In order to explain the influence of the different plasma parameters on the protective properties of SiO_x thin films, the experimental data are fitted by considering a simple equivalent circuit, as shown in Fig. 13 and Table 5 which illustrate constituents of the equivalent circuit. The parameter used to estimate the protection efficiency τ (%) for different films is calculated from the following equation: $\tau = 100 * (R_t - R_{t,0})/R_t$ (Ref 40).

The shown equivalent circuit illustrates constituents of the equivalent circuit as a result of the various deposition

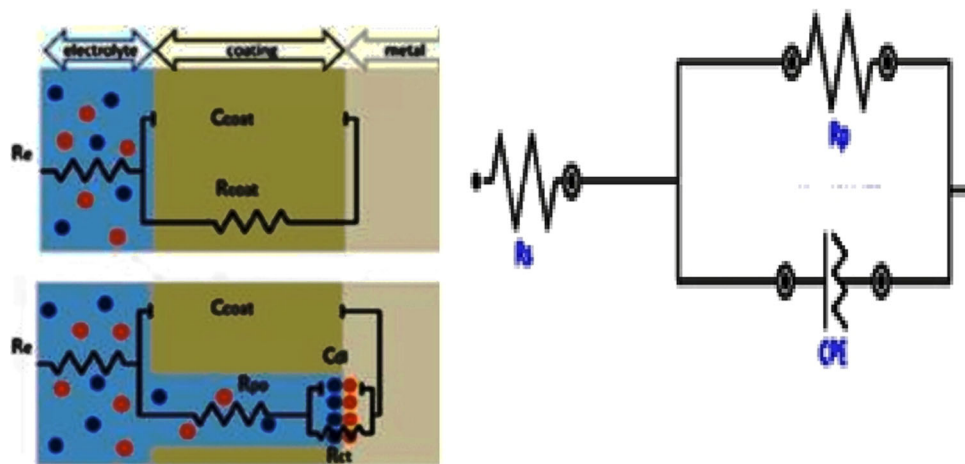



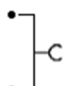


Fig. 13 Equivalent circuit and a classical model used to simulate the coating /substrate systems

Table 5 Illustrates the constituents of the Equivalent circuit

Symbol	Symbol abbreviation	Element
	(Rp)	Polarization resistance* of the corrosion process on the metal/alloy substrate
	(Rs)	Solution resistance** (electrolyte) corresponding to the resistance of the electrolyte
	CPE	Constant Phase Element (shows the inhomogeneous character of the system, frequently considered as electrode roughness and related to the capacitance (Q))
	...	Parallel join connection

*Polarization Resistance (Rp): The corrosion rate of the metal substrate beneath the coating is described by the polarization resistance. For a metal in the absence of a coating, the corrosion rate can be determined from the polarization resistance. The polarization resistance is inversely proportional to the corrosion rate.

**Solution Resistance (Rs): The resistance of the electrolyte between the working electrode and reference electrode. For studies of organic coatings, the electrolyte is very conductive, so Rs is usually very low and can be ignored (Ref 41).

parameters, which served as the foundation for the interpretation of the experimental EIS data.

As seen in Fig. 14 and Table 6, the Nyquist or bode plots of each coating film in use are very similar to those of bare metal. The size of the impedance spectra demonstrates a significant improvement in the corrosion resistance of the metal surface.

By fitting the experimental data to a straightforward equivalent circuit that fits the experimental data and consists of either a one-time constant model, the impedance spectra of the various Nyquist plots were analyzed. The increase in the deposited thin film at 200 power and preactivated with oxygen plasma may be due to the increase in the surface coverage by the deposited molecules. The above-mentioned results can be explained in terms of the deposited layer on the silver-copper alloy substrate producing a chemically protective barrier that hinders the process of charge transfer and hence slows down corrosion reactions and causes Rp value to rise. The increased surface covering by the deposition molecules may be the cause of the efficiency of the thin film that is being deposited at 200 w

and being preactivated with oxygen plasma. The deposited layer on the silver-copper alloy substrate creates a chemically protective barrier that impedes the process of charge transfer, which slows corrosion processes and raises the Rp value. This is how the results above may be explained. The corrosion rate reduces with increased power and without preactivation as the Nyquist plot's diameter increases. Additionally, the electrical double layer at the electrode/solution interface is reduced by the species of the adsorbed and deposited layers.

According to the interpretation of the Bode plot as shown in Fig. 14(b), coated samples show significantly better corrosion resistance than bare substrates, which is demonstrated by higher values of the low-frequency complex impedance (IZI), which can be calculated from the plateau region on the Bode plot in the frequency range of 0.001-0.01 Hz.

By using the Bode plot, it is possible to establish the system's equivalent electric circuit without having to go through the laborious and time-consuming data-fitting processes that are often required. High IZI values are indicative of

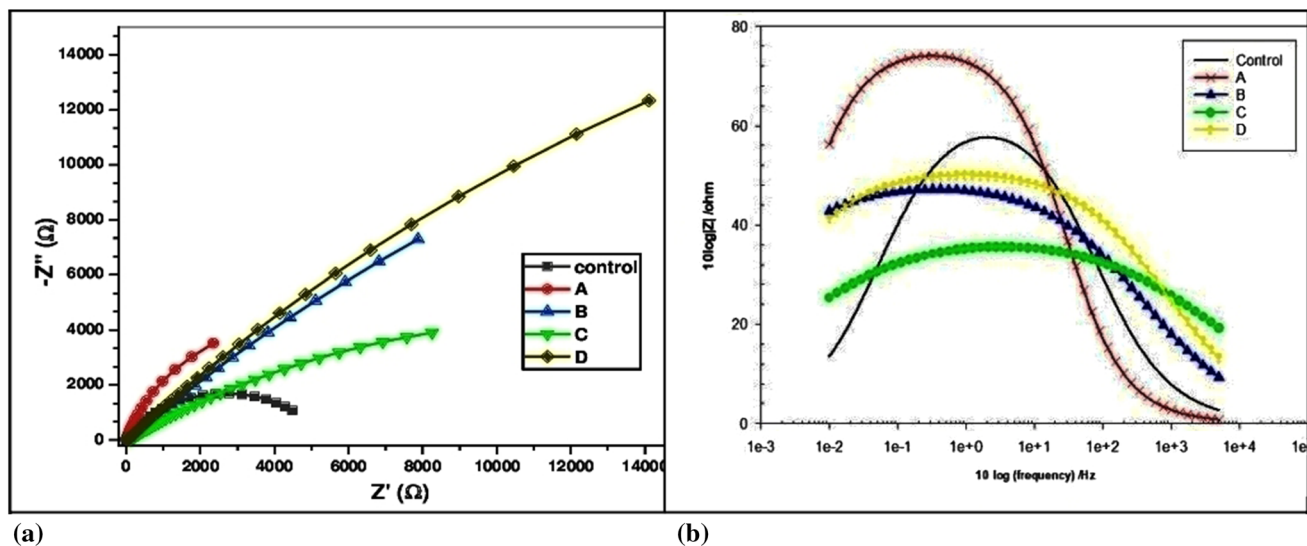


Fig. 14 Nyquist plots (a) and Bode plots (b) of EIS measured in 0.1 M NaCl solution of metal plasma-coated films compared to the bare metal

Table 6 Polarization resistance and the efficiency of deposition films at different conditions

Samples	Rs* Ω	CPE		Rp k Ω	chi- square values	(IE)%	θ
		Y0, $\mu\text{Mh}0$	n1				
Blank	27.2	414	0.72	5.32	0.29815
A	5.77	2.12	0.849	11.9	0.0214	55.29	0.5529
B	37.0	381	0.545	75.3	0.12034	92.93	0.9293
C	48.8	248	0.428	25.0	0.61333	78.72	0.7872
D	32.2	220	0.575	80.4	0.019268	93.38	0.9338

Rs: Solution resistance (electrolyte) (Ω), CPE: Constant Phase Element, Y0: is a proportional factor (μMho), n1 is the phase change values obtained from the fitting, Rp: Polarization resistance of the corrosion process on the alloy substrate (Ω), IE: Efficiency %.

good protective efficiency of the coating; they measure the extent of the electrolytic conduction channels at the metal/coating interface. When applied to clean, uncoated surfaces, IZI is roughly equivalent to polarization resistance, which is correlated with the rate of metal corrosion: the higher the IZI value, the greater the corrosion resistance (Ref 42).

The arrangement of the efficiency of the different deposition conditions is as follows: Coupons with pre-activation and deposited with oxygen plasma at 200 w (sample D) > coupons without pre-activation and deposited with oxygen plasma at 200w (sample B) > coupons with pre-activation and deposited with oxygen plasma at 100 w > coupons without pre-activation and deposited with oxygen plasma at 100w > blank. From the results that were presented to the samples with different deposition conditions, it was found that the sample on which no films were deposited is the lowest in resistance and recorded a lower polarization resistance value ($R_p = 5.32$ k Ω) if compared to the rest of the other samples, while the sample A with a polarization resistance ($R_p = 11.9$ k Ω) and has a protection efficiency about 55.29%, then the sample C with a polarization resistance ($R_p = 25.0$ k Ω) and has a protection efficiency about 78.72%, then the sample B with a polarization resistance ($R_p = 75.3$ k Ω) and has a protection efficiency about 92.93%, while the sample D achieved the best protective efficiency of 93.38% with a polarization resistance ($R_p = 80.4$

k Ω) and has a protection efficiency about 93.38%. Accordingly, these results showed the role of oxygen in the pre-treatment as well as the role of selected applied power. R_p increases by four orders of magnitude if the substrate is previously treated in an O_2 plasma (Ref 43). This demonstrates that the coating and substrate are interfacially bonded. The findings also show that the oxygen plasma treatment improves the adhesion of the substrate to the coating layer.

The increase in the protective efficiency of the PECVD-deposited films is related to the progressive growth of their inorganic nature, i.e., to the increase in the number of SiO_x groups, as shown by comparing the electrochemical characterization of the coating results with the FTIR data. In light of this, it can be said that input power, in addition to oxygen plasma pretreatment, influences the PECVD film's characteristics. There is significant improvement in adhesion by increasing the input power during deposition. Furthermore, this causes the precursor molecule to fragment more frequently (Ref 33). Therefore, increasing the input power lowers the concentration of $SiOH$ as well as the concentration of the other organic groups (Ref 34). Low-supplied power prevents the precursor from being sufficiently ionized and fragmented, and optimum-supplied power results in excessive fragmentation (Ref 44).

4. Conclusion

The following conclusions can be drawn:

- The gaseous precursor partially dissociates in the presence of plasma, the radicals adhere to the surface of metal and/or alloy subjected to plasma, and build amorphous SiO_x layers that are highly effective at preventing corrosion. The concentrations of these components in the deposited film varied considerably depending on the experimental conditions.
- In this work, depositing the siloxane onto silver, pre-treated in plasma according to the variables outlined in the methodology as variations in the plasma process parameters have a significant impact on the corrosion protection capabilities of the SiO_x thin films that are formed on silver copper alloy substrates.
- The input power has an impact on the characteristics of the PECVD film in addition to oxygen plasma pretreatment. An increase in the discharge input power results in the formation of more inorganic films in the SiO_x film's adhesion, an increase in the degree of surface contamination, and a noticeable improvement in the network cross-linking. It also causes a marked increase in the protective effect of the coatings.
- As FTIR and SEM proved, increasing the discharge input power variable during deposition reduced the carbon content of the film and increased its inorganic nature.
- The fabricated coats improved protective properties, as assessed by EIS and by tarnishing test of the coated silver by sulfur dioxide. From the EIS results, it was found that the deposited film improved the protective efficiencies from 55.29 to 92.93%, respectively. The performance is enhanced after the oxygen plasma pretreatment step, and the input power is increased compared to untreated samples.
- The SiO_x film's ability to act as a barrier against the aggressive environment as well as its high conformability to the surface, even when it is already covered in a thin layer of corrosion products, can be linked to the increase in the impedance modulus' ($|Z|$) value.
- The SiO_x film evens out the patina's voids, preventing corrosive species from penetrating through the corrosion layer to the metal's surface.
- Another important consideration for meeting the demands of curators working on the conservation of prehistoric silver artifacts with very intricate embellishments is the high degree of tolerance to any surface roughness.

Acknowledgments

We would like to express our heartfelt appreciation to the anonymous reviewers, whose suggestions significantly improved this work.

Authors' Contributions

Conceptualization: YAE, WAM and MMR; investigation: YAE, WAM and NNM methodology: YAE, WAM, MMR and NNM analysis: YAE; software: NNM, NAAG and KHM; data prepara-

tion: YAE, NAAG and NNM; writing—original draft preparation: YAE, review and editing visualization: YAE, MMR, NAAG and NNM; supervision: WAM, MMR, NNM. All authors read and approved the final manuscript.

Funding

Open access funding provided by The Science, Technology & Innovation Funding Authority (STDF) in cooperation with The Egyptian Knowledge Bank (EKB). This research was not funded (not applicable).

Availability of Data and Materials

Data are available on request from the authors.

Conflict of interest

The authors claim there is no conflict of interest.

Open Access

This article is licensed under a Creative Commons Attribution 4.0 International License, which permits use, sharing, adaptation, distribution and reproduction in any medium or format, as long as you give appropriate credit to the original author(s) and the source, provide a link to the Creative Commons licence, and indicate if changes were made. The images or other third party material in this article are included in the article's Creative Commons licence, unless indicated otherwise in a credit line to the material. If material is not included in the article's Creative Commons licence and your intended use is not permitted by statutory regulation or exceeds the permitted use, you will need to obtain permission directly from the copyright holder. To view a copy of this licence, visit <http://creativecommons.org/licenses/by/4.0/>.

References

1. A.E. Marquardt et al., Protecting Silver Cultural Heritage Objects with Atomic Layer Deposited Corrosion Barriers, *Herit. Sci.*, 2015, **3**(1), p 1–12
2. A. Artesani et al., Recent Advances in Protective Coatings for Cultural Heritage—An Overview, *Coatings*, 2020, **10**(3), p 217
3. C.A. Grissom et al., Evaluation of Coating Performance on Silver Exposed to Hydrogen Sulfide, *J. Am. Inst. Conserv.*, 2013, **52**(2), p 82–96
4. P. Predko et al., Promising Methods for Corrosion Protection of Magnesium Alloys in the Case of Mg-Al, Mg-Mn-Ce and Mg-Zn-Zr: A Recent Progress Review, *Metals*, 2021, **11**(7), p 1133
5. M. Awang, A.A. Khalili, and S.R. Pedapati, A Review: Thin Protective Coating for Wear Protection in High-Temperature Application, *Metals*, 2020, **10**(1), p 42
6. Y. Wang et al., Microstructure and Corrosion Resistance of Ceramic Coating on Carbon Steel Prepared by Plasma Electrolytic Oxidation, *Surf. Coat. Technol.*, 2010, **204**(11), p 1685–1688
7. D. Watkinson, 4.43 Preservation of Metallic Cultural Heritage. Corrosion Management, 2010: p. 3307–3340
8. M. Macgregor and K. Vasilev, Perspective on Plasma Polymers for Applied Biomaterials Nanoengineering and the Recent Rise of Oxazolines, *Materials*, 2019, **12**(1), p 191
9. R. Thirumdas, C. Sarangapani, and U.S. Annature, Cold Plasma: A Novel Non-thermal Technology for Food Processing, *Food Biophys.*, 2015, **10**(1), p 1–11
10. T. Homola et al., Plasma Treatment of Glass Surfaces Using Diffuse Coplanar Surface Barrier Discharge in Ambient Air, *Plasma Chem. Plasma Process.*, 2013, **33**(5), p 881–894

11. A. Patelli, et al. A Customised Atmospheric Pressure Plasma Jet for Conservation Requirements. in IOP Conference Series: Materials Science and Engineering. 2018. IOP Publishing
12. F.S. Madani and M. Hadian Dehkordi, An Overview of the Application of Plasma Technology in the Protection of Cultural and Historical Objects, *J. Res. Archaeom.*, 2018, **4**(1), p 81–94
13. O.O. Abegunde et al., Overview of Thin Film Deposition Techniques, *AIMS Mater. Sci.*, 2019, **6**(2), p 174–199
14. D. Jameel, Thin Film Deposition Processes, *Int. J. Modern Phys. Appl.*, 2015, **1**, p 193–199
15. T. Török, P. Urbán, and G. Lassú, Surface Cleaning and Corrosion Protection Using Plasma Technology, *Int. J. Corros. Scale Inhib.*, 2015, **4**(2), p 116–124
16. Q.H. Trinh et al., Deposition of Superhydrophobic Coatings on Glass Substrates from Hexamethyldisiloxane Using a kHz-Powered Plasma Jet, *Surf. Coat. Technol.*, 2019, **361**, p 377–385
17. G. Lazzara and R.F. Fakhruddin, *Nanotechnologies and Nanomaterials for Diagnostic, Conservation and Restoration of Cultural Heritage*, Elsevier, New York, 2018
18. E. Angelini et al., Surface Analysis of SiO₂-Like High-Barrier Thin Films for Protection of Silver Artefacts, *Surf. Interface Anal.*, 2010, **42**(6–7), p 666–670
19. S. Lovascio, Cold Plasma Deposition of Organosilicon Films with Different Monomers in a Dielectric-Barrier Discharge. 2010, Université Pierre et Marie Curie-Paris VI
20. E. Angelini and S. Grassini, Plasma treatments for the cleaning and protection of metallic heritage artefacts, *Corrosion and Conservation of Cultural Heritage Metallic Artefacts*. Elsevier, 2013, p 552–569
21. N. Σωτηρίου, Low Temperature Plasma Enhanced Chemical Vapor Deposition of Graphene Layers. 2017
22. H. Rauscher, M. Perucca, and G. Buyle, *Plasma Technology for Hyperfunctional Surfaces: Food, Biomedical and Textile Applications*, Wiley, New York, 2010
23. V. Jankauskaitė, P. Narmontas, and A. Lazauskas, Control of Polydimethylsiloxane Surface Hydrophobicity by Plasma Polymerized Hexamethyldisilazane Deposition, *Coatings*, 2019, **9**(1), p 36
24. K. Zuber, R. Radjef, and C. Hall, Dynamic Effects in Siloxane PECVD Coatings, *Front. Nanosci.*, 2019, **14**, p 141–179
25. R.C. Rangel, N.C. Cruz, and E.C. Rangel, Role of the Plasma Activation Degree on Densification of Organosilicon Films, *Materials*, 2020, **13**(1), p 25
26. T. Krueger, L. Hansen, and H. Kersten, Deposition of SiO_x Thin Films Using Hexamethyldisiloxane in Atmospheric Pressure Plasma Enhanced Chemical Vapor Deposition, *J. Phys. Conf. Ser.*, 2020, **1492**, p 012023
27. Ž. Gosar et al., Deposition of SiO_xCyHz Protective Coatings on Polymer Substrates in an Industrial-Scale PECVD Reactor, *Coatings*, 2019, **9**(4), p 234
28. S. Saloum et al., Effect of Surface Modification on the Properties of Plasma-Polymerized Hexamethyldisiloxane Thin Films, *Surf. Interface Anal.*, 2019, **51**(7), p 754–762
29. X. Yan et al., In Situ Surface Modification of Paper-Based Relics with Atmospheric Pressure Plasma Treatment for Preservation Purposes, *Polymers*, 2019, **11**(5), p 786
30. American Society for Testing and Materials (ASTM International), Annual Book of ASTM Standards, Section 3, Metals Test Methods and Analytical Procedures, G 1–90: 2003, Standard Practice for Preparing, Cleaning and Evaluating Corrosion Test Specimens, P.34
31. F. Benitez, E. Martinez, and J. Esteve, Improvement of Hardness in Plasma Polymerized Hexamethyldisiloxane Coatings by Silica-Like Surface Modification, *Thin Solid Films*, 2000, **377**, p 109–114
32. A. Sonnenfeld et al., Deposition Process Based on Organosilicon Precursors in Dielectric Barrier Discharges at Atmospheric Pressure—A Comparison, *Plasma Polym.*, 2001, **6**(4), p 237–266
33. A.N. Chifen et al., Adhesion Improvement of Plasma-Polymerized Maleic Anhydride Films on Gold Using HMDSO/O₂ Adhesion Layers, *Plasma Processes Polym.*, 2007, **4**(9), p 815–822
34. R. d'Agostino et al., Protection of Silver-Based Alloys from Tarnishing by Means of Plasma-Enhanced Chemical Vapor Deposition, *Plasma Processes Polym.*, 2005, **2**(2), p 91–96
35. M. Mozetič, Plasma-Stimulated Super-Hydrophilic Surface Finish of Polymers, *Polymers*, 2020, **12**(11), p 2498
36. F. Fracassi et al., Application of Plasma Deposited Organosilicon Thin Films for the Corrosion Protection of Metals, *Surf. Coat. Technol.*, 2003, **174**, p 107–111
37. J. Batey and E. Tierney, Low-Temperature Deposition of High-Quality Silicon Dioxide by Plasma-Enhanced Chemical Vapor Deposition, *J. Appl. Phys.*, 1986, **60**(9), p 3136
38. J. McEwan, M. Scott, and F. Goodwin. The development of an accelerated tarnish test for sterling silver. in 16th International Corrosion Congress, Beijing. 2005. 3136–3145
39. M.J. Ross, Impedance Spectroscopy, *Ann. Biomed. Eng.*, 1992, **20**, p 289–305
40. E. Cano and B.R. Barat, Electrochemical techniques for in situ corrosion evaluation of cultural heritage, *Advanced Characterization Techniques, Diagnostic Tools and Evaluation Methods in Heritage Science*. D.M. Bastidas, E. Cano Ed., Springer, Berlin, 2018, p 24–26
41. A. M. A. Alsamurrae, H. I. Jaafer, H. A. Ameen, and A. Q. Abdullah, Electrochemical Impedance Spectroscopic Evaluation of Corrosion Protection Properties of Polyurethane/Polyvinyl Chloride Blend Coatings on Steel, *Am. J. Sci. Ind. Res.* 2011 Vol. 2, No. 5,
42. J.R. McDonald, *Impedance Spectroscopy*, John Wiley & Sons, New York, 1987
43. F. Palumbo, R. d'Agostino, F. Fracassi et al., On Low Pressure Plasma Processing for Metal Protection, *Plasma Process. Polym.*, 2010, **7**, p 802–812
44. S. Zanini et al., Characterisation of SiO_xCyHz thin films deposited by low-temperature PECVD, *Vacuum*, 2007, **82**(2), p 290–293

Publisher's Note Springer Nature remains neutral with regard to jurisdictional claims in published maps and institutional affiliations.